1 **Hyperspectral characterization of freezing injury and its biochemical**

2 **impacts in oilseed rape leaves**

3 Chuanwen Wei[a,c], Jingfeng Huang[a,c,*], Xiuzhen Wang[d], George Alan Blackburn[e], Yao Zhang[a,b], Shusen

4 Wang[f], Lamin R. Mansaray[a,c,g]

5 [a] Institute of Applied Remote Sensing and Information Technology, Zhejiang University, 310058 Hangzhou,

6 China

7 [b] Key Laboratory of Environment Remediation and Ecological Health, Ministry of Education, College of

8 Natural Resources and Environmental Science, Zhejiang University, 310058 Hangzhou, China

9 [c] Key Laboratory of Agricultural Remote Sensing and Information Systems, Zhejiang Province, China,

10 Zhejiang University, 310058 Hangzhou, China

11 [d] Institute of Remote Sensing and Earth Sciences, Hangzhou Normal University, 311121 Hangzhou, China

12 [e] Lancaster Environment Centre, Lancaster University, Lancaster, UK

13 [f] Canada Centre for Remote Sensing, Natural Resources Canada, Ottawa, ON, Canada

14 [g] Department of Agro-meteorology and Geo-informatics, Magbosi Land, Water and Environment Research

15 Centre (MLWERC), Sierra Leone Agricultural Research Institute, Tower Hill, Freetown, PMB 1313,

16 Sierra Leone

17 [*] Corresponding author at: Institute of Applied Remote Sensing and Information Technology, Zhejiang

18 University, 310058 Hangzhou, China. Tel.: +86 571 88982830.

19 E-mail addresses: weichuanwen@zju.edu.cn (Ch. Wei), hjf@zju.edu.cn (J. Huang).

20 **Abstract:**

21 Automatic detection and monitoring of freezing injury in crops is of vital

22 importance for assessing plant physiological status and yield losses. This study

investigates the potential of hyperspectral techniques for detecting leaves at the stages of

freezing and post-thawing injury, and for quantifying the impacts of freezing injury on

leaf water and pigment contents. Four experiments were carried out to acquire

hyperspectral reflectance and biochemical parameters for oilseed rape plants subjected

to freezing treatment. Principal component analysis and support vector machines were

applied to raw reflectance, first and second derivatives (SDR), and inverse logarithmic

reflectance to differentiate freezing and the different stages of post-thawing from the

normal leaf state. The impacts on biochemical retrieval using particular spectral domains

were also assessed using a multivariate analysis. Results showed that SDR generated the

highest classification accuracy (>95.6%) in the detection of post-thawed leaves. The

optimal ratio vegetation index (RVI) generated the highest predictive accuracy for

changes in leaf water content, with a cross validated coefficient of determination (R^2cv)

of 0.85 and a cross validated root mean square error (RMSEcv) of 2.4161 mg/cm^2.

Derivative spectral indices outperformed multivariate statistical methods for the

estimation of changes in pigment contents. The highest accuracy was found between the

optimal RVI and the change in carotenoids content (R^2_{CV}=0.70 and RMSE$_{CV}$=0.0015

mg/cm^2). The spectral domain 400-900 nm outperformed the full spectrum in the

estimation of individual pigment contents, and hence this domain can be used to reduce

redundancy and increase computational efficiency in future operational scenarios. Our

findings indicate that hyperspectral remote sensing has considerable potential for

characterizing freezing injury in oilseed rape, and this could form a basis for developing

satellite remote sensing products for crop monitoring.

Keywords: hyperspectral reflectance; oilseed rape; freezing injury; detection; estimation; biochemical parameters

1 Introduction

Winter oilseed rape (*Brassica napus* L.) is an important oilseed crop in China. This crop is mainly cultivated in the Yangtze River basin. Because of the impact of cold spells, winter oilseed rape in this region is frequently subjected to freezing injury, which can lead to a significant decrease in yield and product quality (She et al., 2015; Zhang et al., 2008). Similar negative impacts of freezing are experienced by many different crop types globally (Cromey et al., 1998; Lardon & Triboi-Blondel, 1995; Staggenborg & Vanderlip 1996). Freezing injury is a common weather-induced agricultural hazard and refers to plants suffering from damage when temperatures drop below 0°C. When leaves are exposed to freezing temperatures, ice crystals are formed between cells. Cellular dehydration can then occur because of the difference in water potential between the inside and the outside of the cell, which draws cytoplasmic water from the cell to the growing mass of extracellular ice. With the decrease in temperature, more water moves from the cytoplasm to intercellular spaces. Permanent freezing injury is caused when dehydration extends beyond the tolerance of the plant and/or ice produces mechanical pressure.

Traditionally, monitoring of freezing injury relies on visual surveys by technicians in the field. This approach is dependent on having staff with sufficient expertise. It is time consuming and labor-intensive. Thus, a more effective alternative approach is required for detecting freezing injury in vegetation. Hyperspectral remote sensing has been widely used as a nondestructive technique to monitor various biotic and abiotic stress factors

67 across different spatial scales (Galvao et al., 2011; Liu et al., 2002; Penuelas et al., 1993;

68 Sankaran et al., 2010; Strachan et al., 2002). As the process of freezing injury tends to be

69 fast (often within a few hours), it means that if hyperspectral remotely-sensed data are to

70 be of value in monitoring the process, they need to be acquired at a high temporal

71 resolution. However, currently available optical satellite data lack the spectral and

72 temporal resolution required for monitoring freezing injury in real time. Several satellite

73 missions have been planned to generate suitable data. These include the Geostationary

74 Coastal and Air Pollution Events (GEO-CAPE) mission from the USA (Board, 2007),

75 the Geostationary Environment Monitoring Spectrometer (GEMS) mission from Korea

76 (Bak et al., 2013), and the Sentinel-4 mission from Europe (Berger et al., 2012), which

77 will provide appropriate datasets multiple times per day. In this study, spectroradiometer

78 data were acquired in a laboratory setting at the leaf scale to demonstrate the capabilities

79 for monitoring freezing injury using hyperspectral data, an approach that would provide

80 a basis for airborne and space-borne monitoring in future when remote sensing data of

81 higher spatial, spectral and temporal resolutions become available.

82   At the leaf scale, the spectral reflectance characteristics across the visible (400-750

83 nm), near-infrared (750-1300 nm) and shortwave-infrared (1300-2500 nm) ranges are

84 primarily determined by variations in photosynthetic pigment content, leaf structure and

85 water content (Knipling, 1970; Richardson et al., 2002; Slaton et al., 2001) which can be

86 strongly impacted by freezing injury (Gausman et al., 1984; Wang et al., 2016; Wang et

87 al., 2012). Many studies have been carried out on the potential of using hyperspectral

88 techniques in evaluating the quality and safety attributes of food products (e.g. meat and

89   edible fungi) subjected to freeze damage (Gowen et al., 2009; Thyholt & Isaksson, 1997).

90   Gowen et al. (2009) integrated principal components analysis and linear discriminant

91   analysis to differentiate between undamaged and freeze-damaged mushrooms using

92   hyperspectral imaging. Their results indicated that freeze-damaged mushrooms could be

93   classified with high accuracy (>95%) after only 45 minutes of thawing. Other studies

94   have used hyperspectral data to estimate the changes in biophysical or biochemical

95   parameters after freezing injury. Nicotra et al. (2003) examined the impact of freezing

96   stress on the distribution of photosynthetic pigments in *Eucalyptus pauciflora* leaves

97   using a CASI high-resolution hyperspectral imaging system. Their results demonstrated a

98   considerable spatial variation of chlorophyll content over the surface of the lamina, with

99   marked decreases in chlorophyll content approaching the margins and tips of the leaves.

100   However, changes in the hyperspectral characteristics of crops such as oilseed rape during

101   the freezing injury process are yet to be investigated, and the potential of using

102   hyperspectral techniques to identify leaf status and monitor biochemical changes remains

103   unknown.

104   A variety of different analytical techniques have been used to automatically detect

105   and classify plant stress from remotely sensed data. Amongst these techniques, support

106   vector machines (SVMs) are promising machine learning methods which are suitable for

107   remote sensing applications due to their ability to generalize well even with limited

108   training samples (Mantero et al., 2005). SVMs have already been used in land cover

109   classification (Gao et al., 2015; Hong et al., 2015; Zhang et al., 2015), quantifying

110   vegetation stress (Adjorlolo et al., 2015; Behmann et al., 2014) and land cover change

111 detection (Hichri et al., 2013; Hussain et al., 2013; Nemmour & Chibani, 2006).

112 Furthermore, SVMs have been used to estimate plant biophysical and biochemical

113 parameters such as LAI, biomass, pigments and nitrogen contents (Gleason & Im, 2012;

114 Verrelst et al., 2012; Yang et al., 2011; Zhai et al., 2013). Hence, SVMs hold promise as a

115 method for characterizing freezing injury in plants using hyperspectral data.

116   Multi-collinearity is a common problem within hyperspectral data. It results from a

117 large number of highly correlated wave bands. Some techniques have been proposed to

118 reduce the redundancy of hyperspectral data for vegetation applications. Principal

119 component regression (PCR) and partial least square regression (PLSR) can be employed

120 to solve multi-collinearity problems. Many studies have used these techniques to

121 construct predictive relationships between spectral data and vegetation parameters

122 (Adjorlolo et al., 2015; Gonzalez-Fernandez et al., 2015). In order to reduce redundancy

123 in spectral data, some studies have made a comparison between the full spectrum and

124 specific spectral domains (ranges) for estimating vegetation parameters from remotely

125 sensed hyperspectral data using multivariate models (Gonzalez-Fernandez et al., 2015;

126 Darvishzadeh et al., 2008; Huang & Blackburn, 2011). The results indicate that predictive

127 models based on specific spectral domains are superior to models based on the full

128 spectrum. Hence, there is considerable potential for the use of spectral indices,

129 multivariate regression techniques and optimized spectral domains for assessing freezing

130 injury in vegetation using hyperspectral data, and this warrants further investigation.

131   The overall aim of this study is to determine the applicability of leaf spectral

132 reflectance data for detecting the freezing and post-thawing states of oilseed rape and

133　quantifying the biochemical impacts of freezing. The objectives are to (1) characterize the

134　spectral reflectance of oilseed rape leaves during freezing and post-thawing; (2) identify

135　appropriate analytical techniques that can be applied to reflectance spectra to differentiate

136　between normal leaves and leaves at freezing and different stages of post-thawing; (3)

137　establish predictive models based on leaf spectral reflectance measurements for

138　quantifying the changes in leaf water content (ΔLWC), chlorophyll a (ΔChla),

139　chlorophyll b (ΔChlb), and carotenoids (ΔCars) induced by freezing injury.

140　**2 Materials and methods**

141　**2.1 Plant culture and experimental design**

142　　The experiments were conducted at the Campus Experimental Station of Zhejiang

143　University. The seeds were a local commercial variety of oilseed rape (Zheyou No.50).

144　The soil used for this study was paddy soil. The seeds were sown in black plastic pots (18

145　cm diameter ×16 cm height) on October 13, 2013 and October 20, 2014, and were located

146　outdoors. The seedlings were thinned to two plants per pot at the 3-leaf stage. Plants were

147　watered as necessary and fertilizer was applied according to local agronomic practices.

148　Treatments were carried out at the 8 leaf-stage during the 2013-2014 growing season,

149　while treatments were carried out at the initial stage of budding during the 2014-2015

150　growing season. The air temperature profile during the growing period is given in Fig. 1.
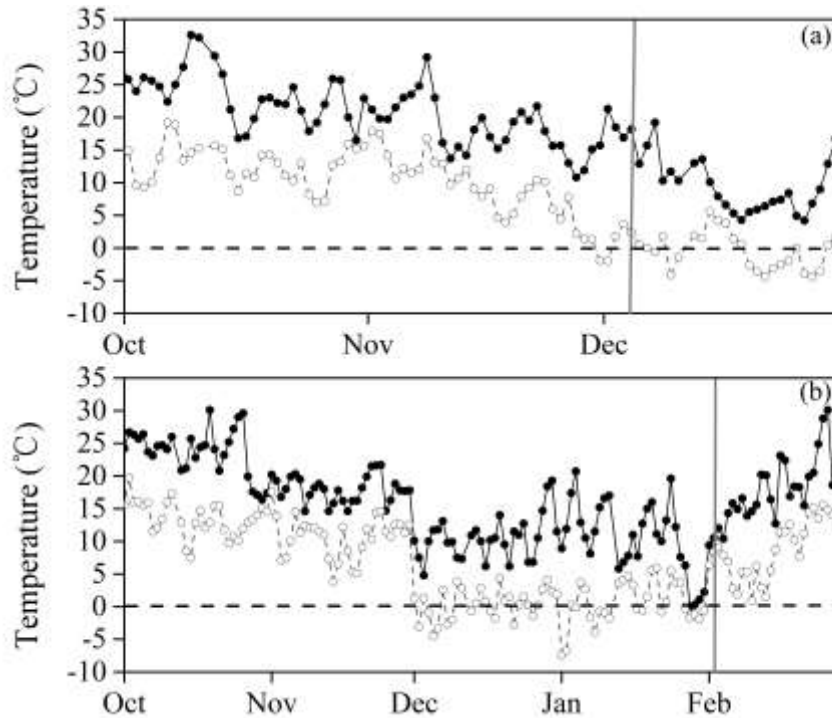
Fig. 1. Minimum and maximum daily temperatures in Hangzhou, China; (a) between October 2013 and December 2013, and (b) between October 2014 and February 2015. The treatment dates are indicated by gray vertical bars. Closed and open circles represent maximum and minimum temperature, respectively.

Each pot containing two plants was transferred to an Aucma freezer (390L in Volume). The freezing of plants was executed under conditions of darkness. Air temperature decreased from laboratory temperature to the lowest temperature range of -10~-12 ℃ . As the formation of rime on the leaves could affect hyperspectral measurements in various ways desiccants were applied to reduce the relative humidity within the freezer during the freezing treatments. Before each measurement, we ensured that there was no rime/frost on the observed leaf surfaces based on visual observation. Leaf temperature was monitored at one second intervals by a digital temperature sensor with a precision of ± 0.5℃ （-10℃～+85℃）. The temperature sensor was connected to

165   a computer on which a 8-channel temperature data acquisition software was installed to

166   log data. The time course of leaf temperature during a typical freezing treatment is shown

167   in Fig. 2. After treatment, the plants were transferred to a light incubator to thaw at 22℃

168   day/18℃ night temperatures with an 11 hour photoperiod (7 am–6 am) and light

169   intensity of 8000 LX.
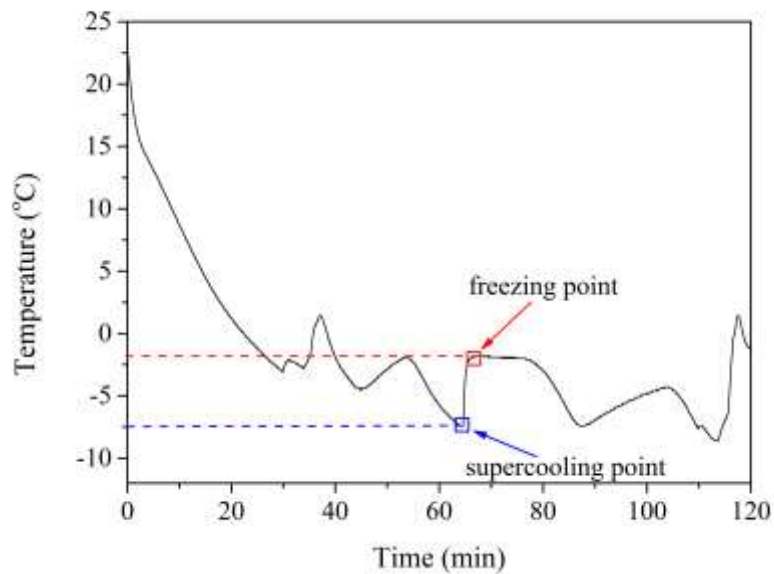
170

171   Fig. 2. Changes of leaf temperature during freezing treatment.

172   *Experiment 1: Changes in cell structure and water content due to freezing.*

173   To determine the effect of freezing on leaf cell structure and water content, 29 pots

174   (samples) were used in this study, with 3 pots treated on each day in the morning,

175   afternoon and night, respectively. A small leaf strip was cut for creating an image of the

176   cross-section in the symmetric right side of the normal leaf. At the same time, three discs

177   were cut from the same side of the leaf with a punch to obtain a measurement of water

178   content. The same procedures were performed on the left side of the leaf 1 hour after the

179   onset of freezing which was detected as a rapid increase in leaf temperature (Brown et al.,

180   1974; Burke et al., 1976).

181   *Experiment 2: Spectral changes over different lengths of freezing.*

182   One leaf sample from a plant was first used to acquire reflectance at the normal

183   state at 8 am. Following the onset of freezing, reflectance of the leaf was measured

184   repeatedly after 10 min, 30 min, 1 hr and then at 1 hr intervals for 10 hrs. Five different

185   plants were measured in this way over a period of 5 days with 1 plant per day.

186   *Experiment 3: Spectral changes during the process of post-thawing.*

187   Spectral reflectance was measured initially on a leaf sample in the normal state at 8

188   pm prior to freezing treatment. When the leaf had been frozen for 1hr, reflectance was

189   measured again. After subjecting the plant to eleven hours of freezing treatment, thawing

190   was initiated and the spectral reflectance of the leaf was measured repeatedly after 2, 4, 6,

191   8, 27, 30, 33, 51, 54 and 57 hrs. Concurrently with each spectral reflectance measurement,

192   a SPAD chlorophyll meter was used to obtain a relative measure of chlorophyll content.

193   In addition, the SPAD values of the leaf in supercooled and frozen states were also

194   measured. The measurement of 26 samples, with 4 pots per day, required a total of 8

195   days.

196   *Experiment 4: Changes in biochemical parameters following thawing.*

197   The spectral reflectance of a leaf in the normal state was measured initially on the

198   left side of the midrib at 8 pm. At the same time, water and pigment contents were

199   measured on the symmetric right side of the leaf by destructive sampling. The plant was

200   then put into the freezer and treated for eleven hours. After post-thawing for two hours in

201   the light incubator, spectral reflectance, water and pigment contents were measured on the

202 left side of the midrib of the leaf. The same procedures were implemented for other leaf

203 samples after post-thawing for 2-58 hrs with an increment of two hours until the leaf

204 became air-dry in the incubator. Three leaves were measured at each time. We expressed

205 the variations in the biochemical parameters as the difference (Δ) between pre and post

206 treatment, which can effectively eliminate the effect of different leaf samples and time

207 variation. The measurement of 29 plants, with 6 pots per day, required a total of 6 days.

208 **2.2 Measurement of leaf reflectance**

209 Leaf reflectance was measured using a FieldSpec 3 spectroradiometer (Analytical

210 Spectral Devices, Boulder, USA) for Experiments 2-4 in 2015. This instrument has a

211 spectral range from 350 to 2500 nm, with a 1.4 nm sampling interval between 350 and

212 1000 nm and 2 nm sampling interval between 1000 and 2500 nm. The spectral

213 resolution of the FieldSpec 3 is 3 nm for the region 350-1000 nm and 8 nm for the region

214 1000-2500 nm. The fiber-optic probe of the spectroradiometer was routed into the

215 freezer so that leaf reflectance measurements could be performed while plants were

216 undergoing treatment, thereby avoiding any disruption to treatment caused by the

217 removal of plants from the freezer for reflectance measurements. The probe was

218 positioned to look down vertically from a height of 3 cm above the leaf, giving a field of

219 view of 1.3 cm^2 at the leaf surface. When measuring leaf reflectance at a particular state,

220 the irradiance incident upon each leaf was first measured by obtaining a radiance

221 spectrum of a white Spectralon panel (Labsphere, North Sutton). The leaf to be

222 measured was then fixed on a lifting platform covered in black cardboard with a round

223 hole of 3 cm in diameter and the leaf was kept at the same height as the white panel

224 surface by adjusting the platform. This setup ensured that the same area of each leaf was

225 repeatedly measured. In order to minimize the impact of background reflectance, a black

226 cover of 2% reflectance was used as the background beneath the leaf. The light source

227 was a 50W quartz halogen lamp which was turned on for the short duration of the

228 reflectance measurements and had no discernable effect on leaf temperature. The angle

229 between the leaf surface and the incident beam was 45°. The interior of the freezer was

230 coated with black material to avoid scattered ambient light. The % reflectance of the leaf

231 was calculated by dividing the leaf radiance by that of the white panel, applying a

232 correction factor for the panel reflectance properties. Ten spectra were recorded and then

233 averaged to represent the leaf reflectance.

234 **2.3 Measurement of biochemical variables**

235 **2.3.1 Chlorophyll and carotenoid contents**

236 In order to acquire the time-series information on chlorophyll content during

237 freezing injury, we employed a nondestructive approach using a SPAD (Minolta, Inc.) to

238 measure the relative chlorophyll content. SPAD readings were taken six times at the leaf

239 margin and their average was considered as the SPAD value of the leaf.

240 For estimating the absolute changes in pigment content, for each leaf sample, three

241 leaf discs (totaling 1.69 cm^2) were obtained using a hole punch, which were then cut into

242 thin strips using scissors. These strips were extracted with 80% acetone in the dark till

243 turning white. The absorbance of the supernatant was measured at 470, 646.8 and 663.2

244 nm with a spectrophotometer (Model UV2550, Shimadzu Corporation, Tokyo, Japan).

245 The contents of chlorophyll a, chlorophyll b and carotenoids were determined using the

246   formulae of Lichtenthaler (1987).

247   **2.3.2 Leaf water content**

248   For each leaf sample, three leaf discs were obtained for the measurement of water

249   content. The fresh weight was measured, after which the discs were dried to a constant

250   mass in an oven at a temperature of 70°C. The leaf water content (LWC) was calculated as

251   follows:

252   LWC= (FM- DM)/A   (1)

253   where, FM is the leaf fresh mass (g), DM is the oven dry leaf mass (g), and A is the area of

254   three leaf discs (cm^2).

255   **2.4 Leaf histology**

256   To examine the cellular structure of normal and frozen leaves, some small strips

257   (approximately 1 mm × 7 mm) were cut from the leaf samples. The specimens were fixed

258   immediately with 3% glutaraldehyde in a 0.015 mol/L phosphate buffer (pH6.9) then air

259   in the strips was pumped out using a syringe until the sections sank to the bottom of a

260   Penicillin bottle. The specimens were put in the refrigerator for more than four hours at

261   4℃. After that, the strips were washed three times in phosphate buffer (0.1M, pH7.0) for

262   15 min at each time. The strips were fixed again using 1% OsO_4 in phosphate buffer

263   (0.1M, pH7.0) for 1-2 hrs, and then washed three times in the same way. The dehydration

264   process was conducted using a graded ethanol series (30%, 50%, 70%, 80%, 90%, 95%,

265   100%) for 15-20 min at each step, and the strips were embedded with Spurr resin

266   following Li and Zhang (2003). Sections of 3-4 μm thickness were sliced using the glass

267   blade on LEICA EM UC7 Ultratome and stained with 0.5% toluidine blue in 0.1% sodium

268   carbonate buffer (pH9.0) for light microscopy, and uranyl acetate and alkaline lead citrate

269   for transmission electron microscopy. Images of the sections were taken using a light

270   microscope (400 × magnification) and a digital camera.

271   **2.5 Data analysis**

272   From all leaf reflectance spectra collected, the wavelength range between 400 nm

273   and 2400 nm was retained for analysis due to high noise levels at both ends of the spectra.

274   The original spectra were then smoothed using a Savitzky–Golay filter with 15 sample

275   points and a second order polynomial (Savitzky & Golay, 1964). The atmospheric water

276   absorption wavebands located at 1350-1480 nm and 1780-1990 nm were also removed

277   from the spectra before further analysis.

278   **2.5.1 Spectral data manipulation**

279   To quantify changes in spectral shape and magnitude with time, we computed the θ

280   and D indices as described by (Price, 1994):

281
$$\theta = \arccos\left(\frac{\sum\limits_{i=1}^{N} S_r * S_s(\lambda_i)}{\left[\sum\limits_{i=1}^{N} S_r^2\right]^{1/2} * \left[\sum\limits_{i=1}^{N} S_s^2(\lambda_i)\right]^{1/2}} \right) \qquad (2)$$

282
$$D = sqrt\left(\frac{\sum\limits_{i=1}^{N} \left(S_r - S_s(\lambda_i)\right)^2}{N} \right) \qquad (3)$$

283   where, λi is the wavelength at band i, N is the number of bands, Ss is the sample

284   spectrum, and Sr is the reference spectrum which is a constant set at 1, representing the

285   maximum of reflectivity. The θ value represents the angle between the reference and the

286   sample spectrum, calculated using a vector dot product. The D value calculates the root

287   mean square difference between the sample spectrum reflectance amplitude and the

288   reference spectrum amplitude.

289   The θ and D indices were calculated for the following wavelength regions: 400 to

290   2400 nm (full spectrum: VIS, NIR, and SWIR), 400 to 750 nm (visible), 751 to 1000 nm

291   (near infrared 1), 1001 to 1350 nm (near infrared 2), 1351 to 1800 (short-wave infrared

292   1), and 1801 to 2400 nm (short-wave infrared 2). The near infrared and the short-wave

293   infrared were divided according to the wavelength limits of individual detectors within

294   the FieldSpec 3 instrument.

295   **2.5.2 Techniques for classification**

296   In addition to using raw spectral reflectance (Raw), the first derivative (FDR),

297   second derivative (SDR) and the inverse logarithm (Log (1/Raw)) of raw reflectance

298   were calculated for discriminating normal leaves from freezing and post-thawing leaves.

299   Derivative techniques can eliminate background signal and separate closely related

300   absorption features (Demetriadesshah et al., 1990). Log (1/Raw) can enhance differences

301   in spectral features in the visible range and reduce the effect of multiplicative factors

302   (Clark & Roush, 1984). We then identified reflectance data that had significant

303   differences between leaves in the normal and freezing 1 hour states and those at different

304   phases of post-thawing by performing mixed effect model analysis with multi-means

305   comparison for all wavebands in the Raw spectra and the various spectral

306   transformations. The nlme package in R software was used to establish the linear mixed

307   effect model and multiple comparisons were conducted using the lsmeans package.

308   Wavebands with a p-value <0.05 were selected as initial candidates. In the final

309   procedure, principal components were used as inputs variables in the SVMs (see section

310   2.5.3) and the number of principal components used was determined according to the

311   criteria of cumulative contribution >90%.

2.5.3 Techniques for retrieval

313   For the retrieval of ΔLWC, five different spectral domains were tested (Table 1). The

314   first was the full spectrum with the atmospheric water vapor absorption wavelengths

315   removed, as these wavelengths cannot be used in space-borne remote sensing. The other

316   four regions were selected based on the description of Jensen (2006), where it was found

317   that the shortwave infrared intervals appear to be more sensitive to changes in plant

318   moisture content than the visible or near infrared portions of the spectrum. For the

319   retrieval of ΔChla, ΔChlb and ΔCars, two domains were tested (Table 1). The first domain

320   was selected by removing atmospheric water absorption wavelengths, while the other was

321   based on the results of Huang & Blackburn (2011) which showed that the spectral

322   wavelength domain 400-900 nm is optimal for quantifying leaf chlorophyll concentration.

323   These spectral domains have been tested and selected in the aforementioned articles and

324   we intended to verify their utility in our study.

325   Table 1. Spectral domains tested for biochemical parameters estimation.

Parameter	Spectral domain
ΔLWC	400-2400 nm, 400-750 nm
	751-1349 nm, 1481-1779 nm
	1991-2400 nm

ΔChla, ΔChlb, ΔCars	400-2400 nm, 400-900 nm

326   We used two methods to estimate the changes in leaf traits based on leaf spectral

327   properties. The first approach correlated spectral vegetation indices (VIs) and measured

328   biophysical parameters. This method has an advantage of fast processing speed. We

329   chose two of the most widely used vegetation indices: ratio index (Jordan, 1969) and

330   normalized difference vegetation index (Rouse et al., 1974) for the estimation of

331   biophysical parameters. To determine the optimal narrow band index, all possible

332   combinations of two bands were calculated and the combination that produced the

333   highest coefficient of determination (R^2) with leaf biophysical parameters was identified.

334   The first derivative reflectance was used to optimize the VIs for ΔLWC and Δpigment

335   content estimation as it exhibited the stronger relationship with the change in

336   biochemical parameters than raw reflectance.

337   In the second approach, the statistical methods PCR, PLSR and SVMs, which

338   exploit information from the full leaf spectrum, were examined. PCR reduces data

339   redundancy by transforming a set of highly correlated variables into a new set of

340   uncorrelated principal components variables (Ye et al., 2008). Both the PCR and PLSR

341   methods have similar structures and are able to avoid the multi-collinearity problem.

342   Whereas PCR performs the decomposition on the spectral data alone, PLSR uses the

343   response variable information during the decomposition process and performs the

344   decomposition on both the spectral data and the response variable simultaneously (Inoue

345   et al., 2012). For PCR, the number of PCs was chosen based on two methods (Mirzaie et

346   al., 2014): (1) percent variance explained in the spectral data and (2) cross-validated

347   RMSE (root mean square error). For PLSR, a leave-one-out cross-validation was

348   employed to determine the number of factors by setting the condition that adding an extra

349   factor must reduce the cross-validated RMSE by >2% (Kooistra et al., 2004). The PCR

350   and PLSR analyses were performed using the pls (Mevik & Wehrens, 2007) package

351   developed in R software (version 3.3.0; Team 2014).

352   SVMs are a supervised machine learning method. The basic theory behind SVMs is

353   to seek the optimal separating hyperplane with the maximum margin, which is the goal

354   of statistical learning theory. In contrast to parametric regression methods in which

355   explicit relationships between spectral observations and biophysical variables are

356   obtained, SVMs provide excellent generalization capabilities, are fast, robust to high

357   input space dimensions and low numbers of samples. SVMs provide sparse solutions

358   where only the most relevant samples of the training data are weighted, resulting in low

359   computational cost and memory requirements. We performed a C-SVC (support vector

360   classification) by minimizing the following objective function (Boser, 1992; Cortes &

361   Vapnik, 1995):

362 $$\min_{\omega,b,\varepsilon} \quad \frac{1}{2}\omega^{T}\omega + C\sum_{i=1}^{n}\xi_{i} \qquad (4)$$

363 $$\text{subject to} \quad y_{i}\left(\omega^{T}\phi(X_{i}) + b\right) \geq 1 - \xi_{i,} \qquad (5)$$
$$\xi_{i} \geq 0$$

364   where, ω and b represent the normal vector and bias of the hyperplane, respectively. x_i

365   ϵR^{n} is an m-dimensional feature vector, $y_i \epsilon [-1,1]$ is the class label, i=1,…,n. C >0 is

366   penalty value and $\xi_i \epsilon R^{n}$ is the slack variable that indicates the distance the sample is

367   from the hyperplane passing through the support vectors of the class to which the sample

belongs, and $\Phi(x_i)$ is the mapping function. In addition, we performed an ε-SVR

(support vector regression) for inversion applications, which minimizes the following

error function (Vapnik, 1998):

$$\min_{\omega, b, \xi, \xi*} \quad \frac{1}{2}\omega^T\omega + C\sum_{i=1}^{n}\xi_i + C\sum_{i=1}^{n}\xi_i^* \tag{6}$$

$$\text{subject to} \quad \omega^T\phi(X_i) + b - Z_i \leq \varepsilon + \xi_i, \tag{7}$$

$$Z_i - \omega^T\phi(X_i) - b \leq \varepsilon + \xi_i^*$$

$$\xi_i, \xi_i^* \geq 0, i = 1, \ldots, n.$$

where, $Z_i \in R^1$ is the target output and ε is the insensitive loss function that controls the

approximation error. Given the nonlinear problems, we used the radial basis kernel

function (RBF) to map the feature vectors into a high dimensional space. The RBF has

been shown to be particularly effective in remote sensing applications (Foody & Mathur,

2004) and is defined as:

$$K(X_i, X_j) = \exp\left(-\gamma\|X_i - X_j\|^2\right), \gamma > 0 \tag{8}$$

where, γ is a parameter that controls the width of the kernel and x_j is the unknown

feature vector. The accuracy of SVMs is dependent on the magnitude of the parameters

C and γ. The latter is inversely proportional to the Gaussian kernel width which

determines the computing window of the RBF kernel matrix, while the former controls

the penalty associated with training samples which lie on the wrong side of the decision

boundary. We optimized these two parameters with a five cross-validated grid search

method to avoid over-fitting. The range of C and γ were both [-10, 10] and the steps

used were 0.5 for both SVC and SVR applications. The LIBSVM 3.20 toolbox (Chang &

389   Lin, 2011) was used for the SVMs analyses in the MATLAB environment.

390   **2.5.4 Accuracy evaluation and model performance**

391   Overall accuracy and Kappa coefficient which are the most commonly used indices

392   for accuracy assessment of remote sensing data (Foody, 2002) were chosen to evaluate the

393   accuracy of SVMs for identifying the status of leaves during freezing injury.

394   Approximately, 75% of the samples were used to train the SVMs and the 25% remaining

395   was used for validation. The whole data set was randomly divided 100 times for repeated

396   accuracy assessments and the average values for the indices were used for accuracy

397   evaluation. To evaluate and compare the predictive models for leaf water and pigments,

398   R^2, RMSE and relative error (RRMSE that is RMSE divided by the sample mean) were

399   used as indicators for this study. The method used for model validation was the

400   leave-one-out cross-validation.

401   **3 Results and discussions**

402   **3.1 Biochemical analysis**

403   A paired-sample t-test showed that there was no significant difference in water

404   content between normal and frozen leaves (p=0.648, α=0.05). Fig. 3 shows the changes

405   in SPAD values for oilseed rape leaves at the stages of supercooling, freezing and

406   post-thawing. As indicated in this figure, the paired-sample t-test also confirmed that

407   there was no significant difference in relative chlorophyll content between normal and

408   frozen leaves (p=0.056, α=0.05). However, there was a significant decline in relative

409   chlorophyll content after 2 hours of post-thawing. As post-thawing progressed, the

410   SPAD values became more variable across the samples tested. This was due to the wide

411   uncertainty in SPAD measurements.
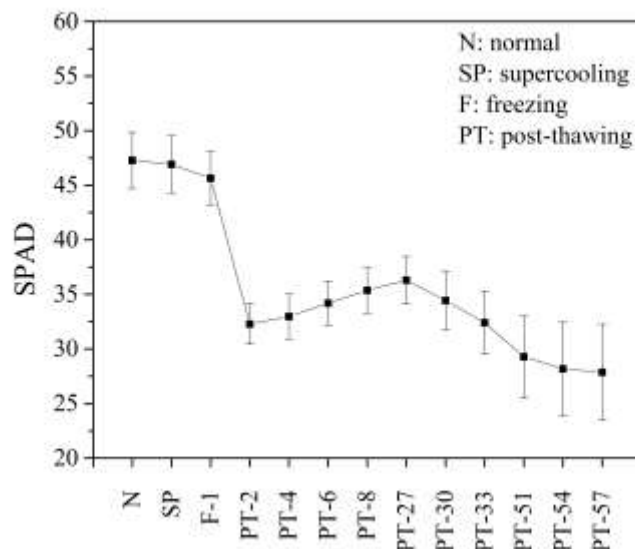

412

413   Fig. 3. Average SPAD values of oilseed rape leaves at the normal, supercooling, 1hr of freezing and at

414   different hours of post-thawing. The bars represent ± 95% confidence interval (CI) (n=26).

415   **3.2 Structural changes of mesophyll cells**

416   Cross-sections of normal and freeze-damaged oilseed rape leaves are presented in

417   Fig. 4. In the normal leaf, the mesophyll cells are turgid and the chloroplasts are arranged

418   along the cell walls (Fig. 4a). A more detailed electron micrograph is shown in Fig. 4c.

419   When plant tissues are subjected to freezing temperatures, ice commonly forms in the

420   intercellular spaces due to the higher freezing point than that in the cytoplasm (Croser et

421   al., 2003; Xin & Browse, 2000). Because of ice formation, the water potential outside the

422   cell drops, which can lead to cellular dehydration and therefore, cell collapse (Guy, 1990).

423   This effect is demonstrated in Fig. 4b for the freeze-damaged leaf, where cell walls have

424   become irregular and the proportion of intercellular air-spaces has increased due to cell

425   contraction. The internal structures of cells such as organelles and plasma membrane have

426   been severely disrupted (Fig. 4d).
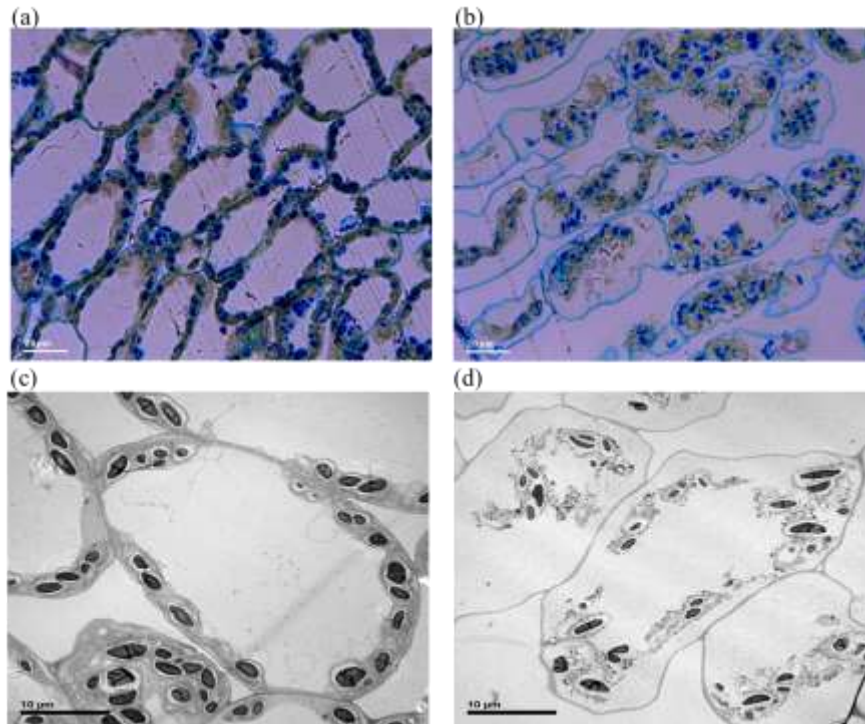
Fig. 4. Light microscopic images (a, b) and transmission electron micrographs (c, d) showing

transverse section of normal (a, c) and freeze-damaged (b, d) oilseed rape leaves.

3.3 Leaf spectral reflectance

Changes in the spectral reflectance of leaves during freezing are depicted in Fig. 5a.

It can be observed that reflectance decreases gradually with the duration of freezing. The

water absorption features shifted gradually to longer wavelengths until all the water inside

the leaf became frozen. D and θ, calculated from different wavelength intervals revealed

the temporal trends of local spectral domains (Fig. 6 (a-f)). D gradually increased over

time for all wavelength domains until the values remained relatively constant. θ values

were generally constant for most of the spectral range except SWIR1 which increased at

first then remained constant after 30 min of freezing. Increasing D values represents a

decrease in reflectance magnitude, while decreasing θ represents a flattening of the

spectral shape.

441   Because the SPAD values and water content displayed no significant changes

442   between normal and frozen leaves (see section 3.1), we surmised that the changes in

443   reflectance were mainly attributable to modifications in cellular structure. As seen from

444   the microscopy (Fig. 4), freezing injury was manifested as a disruption of cell wall

445   configuration, increase in intercellular spaces and disintegration of cell contents which are

446   likely to result in alterations of the refractive index within the leaf and a decrease in

447   scattering of incident light. These changes contributed to the decrease of leaf reflectance

448   throughout the spectrum. Because the peaks in the absorption coefficient of ice are at

449   longer wavelengths than those of liquid water (Green et al., 2006), the positions of the

450   water absorption features in leaf reflectance spectra shift to longer wavelengths when leaf

451   water is transformed into ice upon freezing. In the case of the first strong water absorption

452   feature, the wavelength corresponding to the minimum reflectance moved from 1456 nm

453   to 1486 nm as leaves moved from the normal state to being frozen for 10 minutes. After

454   the leaves were frozen for an hour, the movement of the water absorption feature became

455   much smaller (<5 nm). As we can see from Fig. 5a, a spectral peak at about 750 nm

456   occurred on the near-infrared shoulder for the frozen leaves. This phenomenon is related

457   to chlorophyll fluorescence (Gamon & Surfus, 1999) which is induced by a sudden

458   conversion of plant tissues from dark-adapted to high light conditions within a few

459   seconds, which is an indicator of photosynthetic performance (Gamon et al., 1990). As

460   the control plants were not incubated in the dark before the reflectance measurements

461   this peak was not detectable for the controls.

462   Fig. 5b reveals the changes in the reflectance of oilseed rape leaves during

post-thawing. In contrast to the frozen leaves, the water absorption features in the spectra

of post-thawed leaves returned to their initial wavelength positions, as in the normal leaf.

Leaf reflectance for all spectral intervals at 2 hours of post-thawing decreased

significantly relative to control leaves (Fig. 6 (g-l)). Reflectance in the visible region

decreased at first, then remained constant, and rapidly increased after 30 hours of

post-thawing. Reflectance generally decreased in the NIR1 region, whereas in the NIR2

region it increased with the duration of post-thawing. For both SWIR1 and SWIR2

domains, D and θ gradually decreased over time after 2 hours of post-thawing. At that

stage of post-thawing, the water absorption bands at 970 nm, 1200 nm, 1450 nm and 1940

nm virtually disappeared and the dry matter absorption features became more prominent,

such as those for lignin, cellulose, starch and protein at 1690 nm , 1900 nm, 2130 nm and

2300 nm (Curran, 1989). Such findings concur with Carter (1991), who demonstrated that

a water deficit can alter cell structure and chemistry such that the leaf reflectance

throughout the 400-2500 nm wavelength range can be affected.
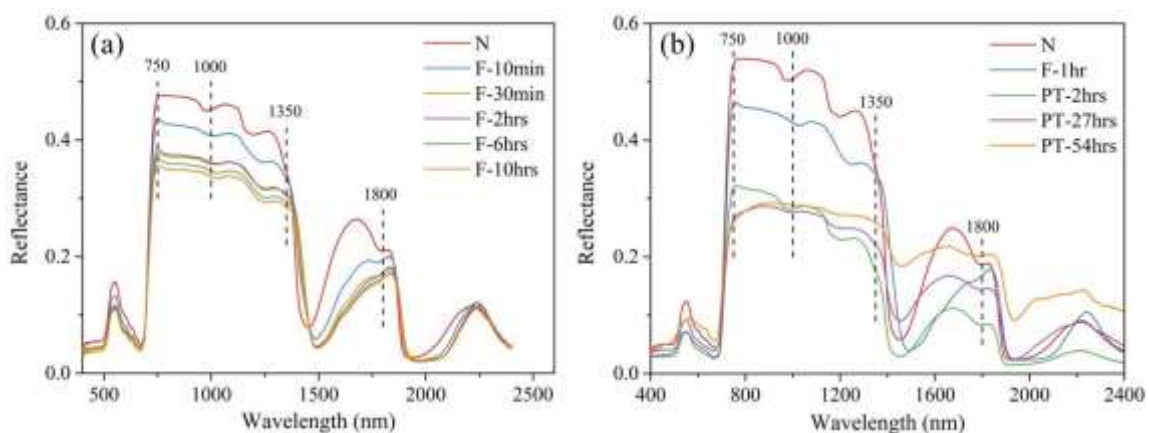
Fig.5. Response of leaf reflectance spectra at different phases of freezing injury: (a) changes in

average reflectance with freezing; (b) changes in average reflectance with post-thawing. N, F and PT

represent normal, freezing and post-thawing in the Legend. Wavelength regions are marked by

481   vertical dashed lines. The total sample sizes are 5 and 26, respectively.
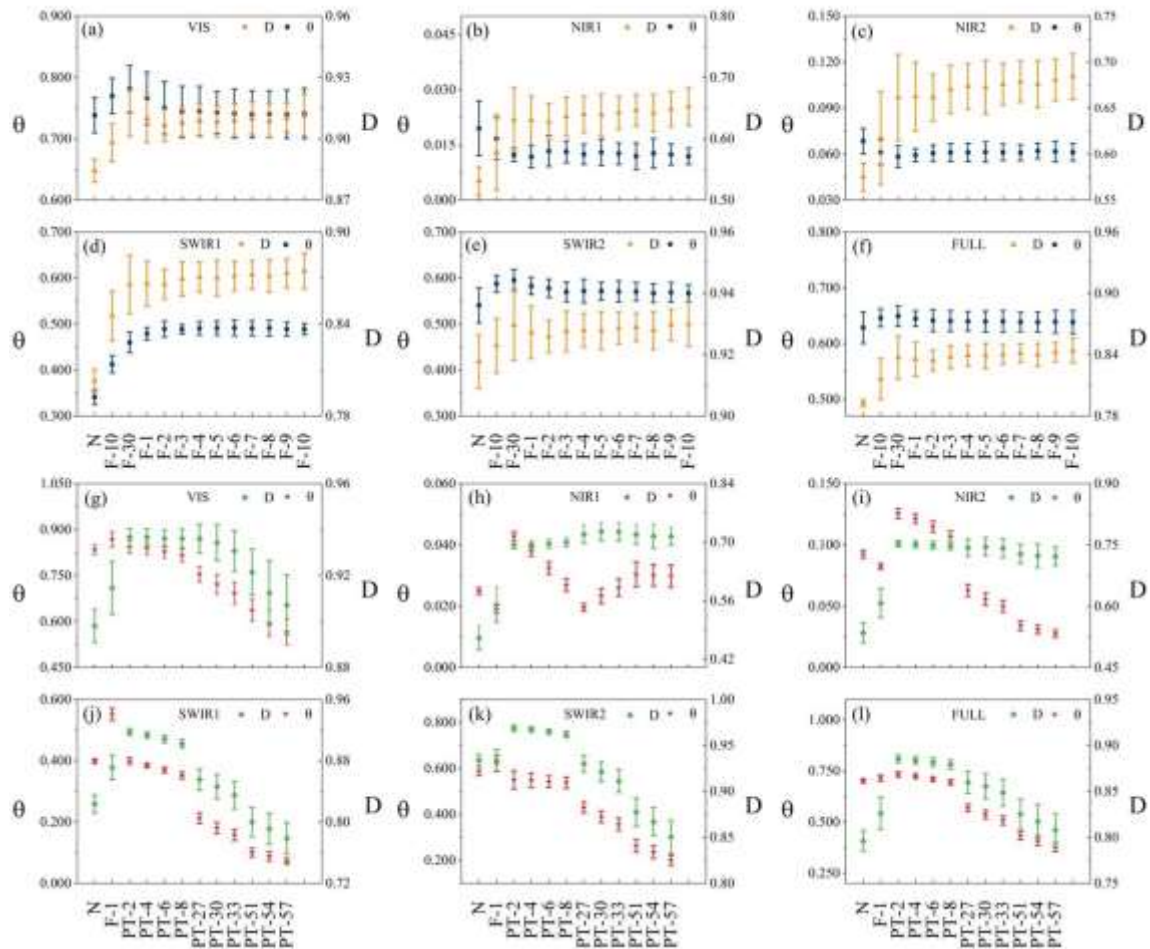
482

483   Fig. 6. Change in indices θ and D; (a-f) during freezing, and (g-l) post-thawing. N represents normal

484   state, F-digit denotes the duration of freezing, PT-digit means the time of post-thawing. Bars

485   represent 95% confidence interval.

486   **3.4 Identification of freezing and the different stages of post-thawing**

487   The identification of leaves frozen for 1hr was effective with an overall

488   accuracy >97.0% for various spectral transformations while the raw reflectance had

489   relatively lower classification accuracy with an overall accuracy of 72.8% (Table 2).

490   These results indicate that the derivative and logarithmic transformations of spectral

491   reflectance were helpful for improving the identification of leaf states during freezing.

492   Although freezing changes water mobility in plant tissues and potentially also pigment

493   content and composition, these are not necessarily lasting effects and some plants could

494   possibly recover. In order to determine whether freezing injury continues, we need to

495   identify further the different stages of post-thawing.

496   Table 2 shows the accuracy with which it is possible to discriminate between

497   normal leaves and leaves that have undergone different durations of post-thawing. The

498   lowest overall classification accuracy for all post-thawing durations is 93.0% based on

499   raw reflectance. These high levels of classification accuracy are due to the fact that the

500   spectral reflectance is significantly different between normal oilseed leaves and those at

501   all stages of post-thawing (see Fig. 5b). In this study, leaves measured in the 2014-2015

502   growing season all became dry and yellow after 3 days of post-thawing. This is

503   attributable to the long duration of freezing treatment (11 hours) and the rapid decrease

504   and subsequent increase in temperature. The heavy freezing injury resulted in large

505   variations of the raw reflectance during post-thawing, thus the classification accuracy

506   was high when using raw reflectance.

507   However, SDR spectra were most effective for discriminating post-thawing leaves

508   with an overall accuracy >95.6%. The overall accuracy based on SDR first reached

509   100% after 33 hrs of post-thawing relative to the other two spectral transformations. The

510   reason for the differences among different transformed spectra types may be that the

511   SDR can better distinguish the similar original spectra by separating the local region

512   with different curvature into several groups (Tsai & Philpot, 1998).

513

514 Table 2. Classification results for the discrimination of normal leaves from leaves at different stages

515 of post-thawing based on raw reflectance and its spectral transformations. OA and KC are overall

516 accuracy and kappa coefficient, respectively. F-digit denotes the duration of freezing, PT-digit means

517 the time of post-thawing.

State (hour)	F-1	PT-2	PT-4	PT-6	PT-8	PT-27	PT-30	PT-33	PT-51	PT-54	PT-57
Raw_OA(%)	72.8	95.0	95.6	97.0	95.6	94.9	95.9	96.1	94.6	93.0	97.9
Raw_KC	0.46	0.90	0.91	0.94	0.91	0.90	0.92	0.92	0.89	0.86	0.96
FDR_OA(%)	98.1	95.3	96.1	96.4	95.9	97.9	98.1	97.9	98.3	98.3	99.5
FDR_KC	0.96	0.91	0.92	0.93	0.92	0.96	0.96	0.96	0.97	0.97	0.99
SDR_OA(%)	99.6	96.2	95.6	97.9	98.4	98.0	99.0	100.0	100.0	100.0	100.0
SDR_KC	0.99	0.92	0.91	0.96	0.97	0.96	0.98	1.00	1.00	1.00	1.00
Log(1/Raw)_OA(%)	97.0	92.7	95.5	96.2	96.1	96.3	97.1	97.9	100.0	100.0	100.0
Log(1/Raw)_KC	0.94	0.85	0.91	0.92	0.92	0.93	0.94	0.96	1.00	1.00	1.00

518 **3.5. Monitoring freezing injury based on the retrieval of leaf biochemical**

519 **parameters from reflectance spectra**

520 **3.5.1 Quantification of biochemicals using hyperspectral vegetation indices**

521 The optimal band combinations and their R^2 values are described in Table 3. Using

522 the 1314 nm and 1642 nm bands, RVI (R^2=0.87) had a stronger linear relationship with

523 ΔLWC than NDVI (0.81) using bands at 1135 and 1697 nm. Similarly, RVI had higher

524 R^2 values (0.68, 0.57, 0.73) than NDVI (0.64, 0.56, 0.65) for ΔChla, ΔChlb, ΔCars,

525 respectively. In previous studies the techniques used here has been applied to find the

526 optimal combination of wavebands using various types of spectral indices for estimating

527   leaf Chla, Chlb (Yu et al., 2014) and water content (Yi et al., 2013), and canopy biomass

528   and LAI (Thenkabail et al., 2000) from a number of species. This study confirms that the

529   method can provide a fast overview of thousands of wavelength combinations and make

530   possible the detection of wavelengths of interest for further analysis.

531   Linear regression models were constructed between the optimal spectral indices and

532   biochemical parameters. The optimal RVI had the highest accuracy in predicting ∆LWC

533   with values of 0.85 for R^2_{CV} and 2.4161 for $RMSE_{CV}$. Ceccato et al. (2002) demonstrated

534   that the SWIR region is sensitive to equivalent water thickness (EWT) but cannot be

535   used alone to retrieve EWT because two other leaf parameters (internal structure and dry

536   matter) also influence leaf reflectance in the SWIR. A combination of SWIR and NIR

537   (only influenced by these two parameters) is necessary to retrieve EWT at leaf level. In

538   our study, although the strong water absorption bands were removed, the selected

539   wavelengths were still located in the NIR and SWIR regions. Reflectance at 1135 and

540   1314 nm had strong linear relationships with ∆LWC (r=-0.88, -0.88, p<0.01) whereas

541   reflectance at 1697 and 1642 nm had relatively lower correlations with ∆LWC (r=-0.44,

542   -0.38, p<0.05). Danson et al. (1992) also obtained a similar finding that the first

543   derivative of the reflectance spectrum at wavelengths corresponding to the slopes on the

544   edges of the water absorption bands was highly correlated with leaf water content and

545   insensitive to differences in leaf structure. In this study, the optimal RVI has a stronger

546   relationship with water than any single reflectance band between 400 to 2400 nm, where

547   the maximum R^2 value was 0.85 for reflectance at 1339 nm.

548   For estimating the changes of pigment content, the optimal RVI provided a higher

549 predictive accuracy than the optimal NDVI (Table 3). The chlorophylls have strong

550 absorption peaks in the red and blue regions of the spectrum. Since the blue peak

551 overlaps with the absorption of carotenoids, it is not generally used for the estimation of

552 chlorophyll content. Maximum absorption in the red region occurs between 660 and 680

553 nm (Sims & Gamon, 2002). However, reflectance at these wavelengths has not proved

554 as useful for predicting chlorophyll content as reflectance at slightly longer or shorter

555 wavelengths. This is because, relatively low chlorophyll contents are sufficient to

556 saturate absorption in the 660–680 nm region. Blackburn (1998) noted that reflectance

557 along the wings of pigment absorption features are optimal in this context as they do not

558 reach saturation but remain sensitive through a range of pigment concentrations and are

559 not convoluted by other pigments. Estimation of leaf carotenoid content from reflectance

560 is much more difficult than estimation of chlorophyll because of the overlap between the

561 chlorophyll and carotenoid absorption peaks and the higher concentration of chlorophyll

562 than carotenoid in most leaves. However, there was a higher predictive accuracy for

563 ΔCars (RRMSEcv=0.3305) in our study compared to ΔChla, ΔChlb (RRMSEcv=0.6724,

564 1.4087). This is because the coefficient of determination between time and ΔCars is 0.49

565 during the post-thawing while the R^2 values of ΔChla (0.40), ΔChlb (0.18) during the

566 post-thawing were relative lower. The optimal wavelength obtained by empirical

567 methods such as regression can be affected by various factors including species, unit and

568 range of pigment concentrations, data acquisition and preprocessing methods, and this

569 may account for some of the disparities between the results presented in different papers.

570 Overall, the results in this study indicate that vegetation indices have the potential to

571   estimate the changes in biochemical parameters that result from freezing injury.

572   Table 3. The optimal band positions for each type of spectral vegetation index and cross-validation

573   results for the accuracy of derived estimates of biochemical contents from the optimal indices.

VIs	Band position and R^2 values			Cross-validated statistics		
	R^2	λ1	λ2	R^2cv	RMSEcv (mg/cm^2)	RRMSEcv
ΔLWC						
NDVI	0.81	1135	1697	0.78	2.9400	0.2208
RVI	0.87	1314	1642	0.85	2.4161	0.1814
ΔChla						
NDVI	0.64	553	636	0.58	0.0044	0.7289
RVI	0.68	641	1295	0.65	0.0041	0.6724
ΔChlb						
NDVI	0.56	2110	2286	0.46	0.0013	1.5368
RVI	0.57	696	2155	0.53	0.0012	1.4087
ΔCars						
NDVI	0.65	648	676	0.61	0.0018	0.3791
RVI	0.73	641	959	0.70	0.0015	0.3305

574   **3.5.2 Quantification of biochemicals using multivariate statistical models**

575   **3.5.2.1 Changes in leaf water content**

576   The predictive accuracy of models for deriving ΔLWC from leaf reflectance spectra

577   using different multivariate techniques is summarized in Table 4. PLSR and PCR

578 performed better than SVMs for the first four spectral domains while the three techniques

579 had similar estimation accuracies in the 1991-2400 nm regions. Although PLSR has an

580 advantage over PCR in theory, in most situations, the methods achieve similar prediction

581 accuracies and PCR usually needs more latent variables than PLSR (Mevik & Wehrens,

582 2007). The quality of SVMs models depends on the selection of kernel functions and the

583 proper setting of hyper-parameters and kernel parameters. Whereas existing sources on

584 SVMs regressions (Smola et al., 1998; Vapnik, 1998) give some recommendations on

585 appropriate settings of SVMs parameters, there is no general consensus and there are

586 many contradictory opinions. In this study, we used the most widely used grid search

587 method to optimize the parameters by artificially specifying the parameters range. Some

588 advanced intelligent optimization algorithms may improve the performance of SVMs

589 such as the genetic algorithm, particle swarm optimization and the simulated annealing

590 algorithm, and these approaches may be worthy of future investigation in the context of

591 this research problem.

592   Amongst the five specific spectral domains tested, the best predictive accuracy for

593 ΔLWC was achieved by using the full spectrum (with atmospheric water absorption

594 bands removed) using PLSR and PCR, which produced the same R^2cv value of 0.85 and

595 the same RMSEcv of 2.4408 (Table 4). The predicted accuracy of ΔLWC using only the

596 751-1349 nm spectral domain in PLSR and PCR was second to the full spectrum with

597 R^2cv and RMSEcv values of 0.81 and 2.7272, respectively. The SWIR wavelength

598 intervals 1481-1779 nm and 1991-2400 nm were superior to the visible region but

599 inferior to the NIR region. The reason for this was that the strong water absorption bands

600   were removed from spectra before analysis in this study. From the perspective of

601   multivariate statistical analysis, the full spectrum domain was optimal for retrieving

602   water content. The optimal sub-spectral region needs further exploration, in order to

603   improve the computational efficiency.

604   Table 4. Cross-validation statistics for predictive models in deriving ΔLWC from leaf spectral

605   reflectance using three multivariate analysis techniques and three different spectral domains.

Spectral domains	Method	R^2cv	RMSEcv (mg/cm^2)	RRMSEcv
400-2400 nm	PLSR	0.85	2.4408	0.1833
	PCR	0.85	2.4408	0.1833
	SVMs	0.72	3.3699	0.2531
400-750 nm	PLSR	6.0E-04	6.5594	0.4926
	PCR	4.7E-02	6.4424	0.4838
	SVMs	3.5E-05	7.6421	0.5739
751-1349 nm	PLSR	0.81	2.7272	0.2048
	PCR	0.81	2.7272	0.2048
	SVMs	0.72	3.6441	0.2737
1481-1779 nm	PLSR	0.74	3.2321	0.2427
	PCR	0.69	3.5293	0.2651
	SVMs	0.62	3.9674	0.2979
1991-2400 nm	PLSR	0.54	4.3279	0.3250
	PCR	0.56	4.2605	0.3200
	SVMs	0.55	4.3614	0.3275

3.5.2.2 Changes in the concentrations of leaf pigments

The predictive accuracy of models for deriving ΔChla, ΔChlb and ΔCars from leaf reflectance spectra using different multivariate techniques is summarized in Table 5. For both spectral domains that were tested, PLSR and PCR had similarly high predictive accuracies for ΔChla and ΔChlb. For ΔCars, PLSR and PCR exhibited similar predictive accuracies when applied to the 400-900 nm domain, whereas for the 400-2400 nm domain, PLSR had a higher predictive accuracy than that of PCR. When comparing the predictive ability of the SVMs to the aforementioned methods, it can be observed that the PLSR method produced superior predictive accuracies over SVMs for all leaf pigments for both spectral domains. SVMs only achieved superiority over the PCR method in the estimation of ΔCars when applied to the 400-900 nm spectral domain. Different methods displayed different levels of effectiveness in the estimation of different biochemical parameters which may be due to variations in the applicability of each algorithm. Similar to the vegetation index results, the estimation accuracies for ΔChlb were poor for all three methods and two spectral domains. This is likely due to the changes in Chlb during post-thawing being minimal ($R^2 = 0.18$).

The estimation accuracy of each technique in the spectral domain 400-900 nm outperformed the full spectrum for the prediction of all three pigments. Although this optimal domain was only proposed for chlorophylls in the study of Huang & Blackburn (2011), this domain is still optimal for all the individual pigments in our study using the three multivariate regression techniques. This confirms that the 400-900 nm region is most informative for the estimation of leaf pigment content.

628 Table 5. Cross-validation statistics in deriving ΔChla, ΔChlb and ΔCars from leaf spectral reflectance

629 using three multivariate analysis techniques and two different spectral domains.

Variable	Method	Spectral domains					
		400-2400 nm			400-900 nm		
		R^2cv	RMSEcv (mg/cm^2)	RRMSEcv	R^2cv	RMSEcv (mg/cm^2)	RRMSEcv
ΔChla	PLSR	0.29	0.0060	0.9836	0.36	0.0056	0.9254
	PCR	0.30	0.0062	1.0171	0.36	0.0056	0.9254
	SVMs	0.09	0.0070	1.1560	0.33	0.0058	0.9452
ΔChlb	PLSR	0.05	0.0019	2.1668	0.06	0.0018	2.0599
	PCR	0.05	0.0019	2.1668	0.06	0.0018	2.0599
	SVMs	0.06	0.0021	2.4141	0.01	0.0020	2.2723
ΔCar	PLSR	0.41	0.0023	0.4883	0.46	0.0021	0.4508
	PCR	0.21	0.0031	0.6638	0.46	0.0021	0.4508
	SVMs	0.38	0.0023	0.4824	0.47	0.0021	0.4450

630 **4**. **Conclusions**

631   In this study, we analyzed the changes in the spectral reflectance of oilseed rape

632 leaves that were subjected to freezing and post-thawing processes. We explored the

633 potential for using changes in spectral reflectance to detect the different stages of the

634 freezing and post-thawing processes, and to quantify the biochemical impacts of freezing

635 injury. The main findings are summarized as follows:

636 (1) The reflectance of leaves shows a significant decrease during freezing and then

637   remains constant across the optical spectrum as the freezing period continues. The

638   most significant spectral characteristic is that water absorption features shift towards

639   longer wavelengths, which is caused by the change of state of leaf water from liquid

640   to solid.

641 (2) In the process of post-thawing, the changes in spectral reflectance of leaves can

642   mainly be attributed to the changing water content of the leaf and the subsequent

643   changes in pigment content and cellular structure.

644 (3) SDR spectra exhibited the highest potential for discriminating leaves at different

645   stages of post-thawing from normal leaves.

646 (4) Derivative spectral indices formulated using optimized narrow wavebands were

647   most effective in quantifying the changes in pigment and water contents of leaves

648   subjected to freezing injury.

649 (5) In freezing injured leaves, the spectral domain 400-900 nm is optimal for

650   developing predictive models of pigment contents. Therefore, selection of this

651   spectral domain for analysis could reduce redundancy and increase computational

652   efficiency in future operational remote sensing scenarios.

653   This study focused on oilseed rape at the leaf scale in a laboratory setting. The results

654 provide evidence to establish the use of spectral reflectance for identifying different

655 stages of freezing injury in crops and quantifying the biochemical impacts of the process.

656 Further work is now needed to develop this capability by investigating freezing injury in

657 other crop species at the canopy and field scales using airborne and spaceborne

658 hyperspectral remotely-sensed data. Such developments have a considerable potential to

659 improve the monitoring and loss evaluation of freezing injury in crops when remotely

660 sensed data of sufficiently high spatial, temporal and spectral resolution are available.

661

667

668 References

669   Adjorlolo, C., Mutanga, O., & Cho, M.A. (2015). Predicting C3 and C4 grass nutrient variability
670 using in situ canopy reflectance and partial least squares regression. *International Journal of Remote*
671 *Sensing, 36*, 1743-1761.

672   Bak, J., Kim, J.H., Liu, X., Chance, K., & Kim, J. (2013). Evaluation of ozone profile and tropospheric
673 ozone retrievals from GEMS and OMI spectra. *Atmospheric Measurement Techniques, 6*, 239-249.

674   Behmann, J., Steinruecken, J., & Pluemer, L. (2014). Detection of early plant stress responses in
675 hyperspectral images. *ISPRS Journal of Photogrammetry and Remote Sensing, 93*, 98-111.

676   Berger, M., Moreno, J., Johannessen, J.A., Levelt, P.F., & Hanssen, R.F. (2012). ESA's sentinel
677 missions in support of earth system science. *Remote Sensing of Environment, 120*, 84-90.

678   Blackburn, G.A. (1998). Spectral indices for estimating photosynthetic pigment concentrations: A test
679 using senescent tree leaves. *International Journal of Remote Sensing, 19*, 657-675.

680   Board, S.S. (2007). Earth science and applications from space: National imperatives for the next
681 decade and beyond. Washington, DC: National Academies Press.

682   Boser, B.E., Guyon, I.M., & Vapnik, V.N. (1992). A training algorithm for optimal margin classifiers.
683 Proceedings of the Fifth Annual Workshop on Computational LearningTheory, p.144-152, Pittsburgh,
684 Pennsylvania, USA.

685   Brown, M.S., Pereira, E.S.B., & Finkle, B.J. (1974). Freezing of nonwoody plant tissues Ⅱ. Cell
686 damage and fine-structure of freezing curves. *Plant physiology, 53*, 709-711.

687   Burke, M.J., Gusta, L.V., Quamme, H.A., Weiser, C.J., & Li, P.H. (1976). Freezing and injury in plants.
688 *Annual Review of Plant Physiology and Plant Molecular Biology, 27*, 507-528.

689   Carter, G.A. (1991). Primary and secondary effects of water content on the spectral reflectance of
690 leaves. *American Journal of Botany, 78*, 916-924.

691   Ceccato, P., Gobron, N., Flasse, S., Pinty, B., & Tarantola, S. (2002). Designing a spectral index to
692 estimate vegetation water content from remote sensing data: Part 1 - theoretical approach. *Remote Sensing*

of Environment, 82, 188-197.

Chang, C.C., & Lin, C.J. (2011). Libsvm: A library for support vector machines. http://www.csie.ntu.edu.tw/~cjlin/libsvm/.

Clark, R.N., & Roush, T.L. (1984). Reflectance spectroscopy quantitative analysis techniques for remote sensing applications. *Journal of Geophysical Research, 89*, 6329-6340.

Cortes, C., & Vapnik, V. (1995). Support vector networks. *Machine Learning, 20*, 273-297.

Cromey, M.G., Wright, D.S.C., & Boddington, H.J. (1998). Effects of frost during grain filling on wheat yield and grain structure. *New Zealand Journal of Crop and Horticultural Science, 26*, 279-290.

Croser, J.S., Clarke, H.J., Siddique, K.H.M., & Khan, T.N. (2003). Low temperature stress: Implications for chickpea (cicer arietinum l.) improvement. *Critical Reviews in Plant Sciences, 22*, 185-219.

Curran, P.J. (1989). Remote sensing of foliar chemistry. *Remote Sensing of Environment, 30*, 271-278.

Danson, F.M., Steven, M.D., Malthus, T.J., & Clark, J.A. (1992). High-spectral resolution data for determining leaf water content. *International Journal of Remote Sensing, 13*, 461-470.

Darvishzadeh, R., Skidmore, A., Schlerf, M., & Atzberger, C. (2008). Inversion of a radiative transfer model for estimating vegetation LAI and chlorophyll in a heterogeneous grassland. *Remote Sensing of Environment, 112*, 2592-2604.

Foody, G.M. (2002). Status of land cover classification accuracy assessment. *Remote Sensing of Environment, 80*, 185-201.

Foody, G.M., & Mathur, A. (2004). A relative evaluation of multiclass image classification by support vector machines. *IEEE Transactions on Geoscience and Remote Sensing, 42*, 1335-1343.

Galvao, L.S., dos Santos, J.R., Roberts, D.A., Breunig, F.M., Toomey, M., & de Moura, Y.M. (2011). On intra-annual EVI variability in the dry season of tropical forest: A case study with MODIS and hyperspectral data. *Remote Sensing of Environment, 115*, 2350-2359.

Gamon, J.A., Field, C.B., Bilger, W., Bjorkman, O., Fredeen, A.L., & Penuelas, J. (1990). Remote sensing of the xanthophyll cycle and chlorophyll fluorecence in sunflower leaves and canopies. *Oecologia, 85*, 1-7.

Gamon, J.A., & Surfus, J.S. (1999). Assessing leaf pigment content and activity with a reflectometer. *New Phytologist, 143*, 105-117.

Gao, L., Li, J., Khodadadzadeh, M., Plaza, A., Zhang, B., He, Z., & Yan, H. (2015). Subspace-based support vector machines for hyperspectral image classification. *IEEE Geoscience and Remote Sensing Letters, 12*, 349-353.

Gausman, H.W., Burke, J.J., & Quisenberry, J.E. (1984). Use of leaf optical properties in plant stress research. *ACS Symposium Series, 257*, 215-233.

Gleason, C.J., & Im, J. (2012). Forest biomass estimation from airborne LiDAR data using machine learning approaches. *Remote Sensing of Environment, 125*, 80-91.

Gonzalez-Fernandez, A.B., Rodriguez-Perez, J.R., Marabel, M., & Alvarez-Taboada, F. (2015). Spectroscopic estimation of leaf water content in commercial vineyards using continuum removal and partial least squares regression. *Scientia Horticulturae, 188*, 15-22.

Gowen, A.A., Taghizadeh, M., & O'Donnell, C.P. (2009). Identification of mushrooms subjected to freeze damage using hyperspectral imaging. *Journal of Food Engineering, 93*, 7-12.

Green, R.O., Painter, T.H., Roberts, D.A., & Dozier, J. (2006). Measuring the expressed abundance of the three phases of water with an imaging spectrometer over melting snow. *Water Resources Research, 42*.

Guy, C.L. (1990). Cold acclimation and freezing stress tolerance: Role of protein metabolism. *Annual Review of Plant Physiology and Plant Molecular Biology, 41*, 187-223.

737   Hichri, H., Bazi, Y., Alajlan, N., & Malek, S. (2013). Interactive segmentation for change detection in
738   multispectral remote sensing images. *IEEE Geoscience and Remote Sensing Letters, 10*, 298-302.

739   Hong, G., Wang, S., Li, J., & Huang, J. (2015). Fully polarimetric synthetic aperture radar (SAR)
740   processing for crop type identification. *Photogrammetric Engineering & Remote Sensing, 81*, 109-117.

741   Huang, J.F., & Blackburn, G.A. (2011). Optimizing predictive models for leaf chlorophyll
742   concentration based on continuous wavelet analysis of hyperspectral data. *International Journal of Remote*
743   *Sensing, 32*, 9375-9396.

744   Hussain, M., Chen, D., Cheng, A., Wei, H., & Stanley, D. (2013). Change detection from remotely
745   sensed images: From pixel-based to object-based approaches. *ISPRS Journal of Photogrammetry and*
746   *Remote Sensing, 80*, 91-106.

747   Inoue, Y., Sakaiya, E., Zhu, Y., & Takahashi, W. (2012). Diagnostic mapping of canopy nitrogen
748   content in rice based on hyperspectral measurements. *Remote Sensing of Environment, 126*, 210-221.

749   Jensen, J.R. (2006). Remote sensing of the environment: An earth resource perspective. (2nd Edition
750   ed.). New Jersey: Prentice Hall, (Chapter 11).

751   Jordan, C.F. (1969). Derivation of leaf area index from quality of light on forest floor. *Ecology, 50*,
752   663-666.

753   Knipling, E.B. (1970). Physical and physiological basis for the reflectance of visible and near-infrared
754   radiation from vegetation. *Remote Sensing of Environment*, 155-159.

755   Kooistra, L., Salas, E.A., Clevers, J.G., Wehrens, R., Leuven, R.S., Nienhuis, P.H., et al. (2004).
756   Exploring field vegetation reflectance as an indicator of soil contamination in river floodplains.
757   *Environmental Pollution, 127*, 281-290.

758   Lardon, A., & TriboiBlondel, A.M. (1995). Cold and freeze stress at flowering: Effects on seed yields
759   in winter rapeseed. *Field Crops Research, 44*, 95-101.

760   Lichtenthaler, H.K. (1987). Chlorophylls and carotenoids: Pigments of photosynthetic biomembranes.
761   *Methods in Enzymology, 148*, 350-382.

762   Liu, Z., Huang, F., Li, L., & Wan, E. (2002). Dynamic monitoring and damage evaluation of flood in
763   north-west jilin with remote sensing. *International Journal of Remote Sensing, 23*, 3669-3679.

764   Mantero, P., Moser, G., & Serpico, S.B. (2005). Partially supervised classification of remote sensing
765   images through SVM-based probability density estimation. *IEEE Transactions on Geoscience and Remote*
766   *Sensing, 43*, 559-570.

767   Mevik, B.H., & Wehrens, R. (2007). The pls package: Principal component and partial least squares
768   regression in R. *Journal of Statistical Software, 18*, 1-23.

769   Mirzaie, M., Darvishzadeh, R., Shakiba, A., Matkan, A.A., Atzberger, C., & Skidmore, A. (2014).
770   Comparative analysis of different uni- and multi-variate methods for estimation of vegetation water content
771   using hyper-spectral measurements. *International Journal of Applied Earth Observation and*
772   *Geoinformation, 26*, 1-11.

773   Nemmour, H., & Chibani, Y. (2006). Multiple support vector machines for land cover change
774   detection: An application for mapping urban extensions. *ISPRS Journal of Photogrammetry and Remote*
775   *Sensing, 61*, 125-133.

776   Nicotra, A.B., Hofmann, M., Siebke, K., & Ball, M.C. (2003). Spatial patterning of pigmentation in
777   evergreen leaves in response to freezing stress. *Plant Cell and Environment, 26*, 1893-1904.

778   Penuelas, J., Filella, I., Biel, C., Serrano, L., & Save, R. (1993). The refectance at the 950-970 nm
779   region as an indicator of plant water status. *International Journal of Remote Sensing, 14*, 1887-1905.

780   Price, J.C. (1994). How unique are spectral signatures?. *Remote Sensing of Environment, 49*, 181-186.

781   Richardson, A.D., Duigan, S.P., & Berlyn, G.P. (2002). An evaluation of noninvasive methods to
782 estimate foliar chlorophyll content. *New Phytologist, 153*, 185-194.

783   Rouse, J.W., Haas, R.H., & Schell, J.A. (1974). Monitoring vegetation systems in the great plains with
784 ERTS, NASA SP-351. Third ERTS-1 Symposium, Vol. 1, pp. 309–317, NASA, Washington, DC.

785   Sankaran, S., Mishra, A., Ehsani, R., & Davis, C. (2010). A review of advanced techniques for
786 detecting plant diseases. *Computers and Electronics in Agriculture, 72*, 1-13.

787   Savitzky, A., & Golay, M.J.E. (1964). Smoothing and differentiation of data by simplified least squares
788 procedures. *Analytical Chemistry, 36*, 1627-1639.

789   She, B., Huang, J.f., Guo, R.f., Wang, H.b., & Wang, J. (2015). Assessing winter oilseed rape freeze
790 injury based on Chinese HJ remote sensing data. *Journal of Zhejiang University Science B, 16*, 131-144.

791   Sims, D.A., & Gamon, J.A. (2002). Relationships between leaf pigment content and spectral
792 reflectance across a wide range of species, leaf structures and developmental stages. *Remote Sensing of
793 Environment, 81*, 337-354.

794   Slaton, M.R., Hunt, E.R., & Smith, W.K. (2001). Estimating near-infrared leaf reflectance from leaf
795 structural characteristics. *American Journal of Botany, 88*, 278-284.

796   Smola, A.J., Murata, N., Schölkopf, B., & Müller, K.R. (1998). Asymptotically optimal choice of
797 ε-loss for support vector machines. Proceedings of the International Conference on Artificial Neural
798 Networks, (pp. 105−110). Berlin: Springer. http://citeseer.ist.psu.edu/26614.html.

799   Staggenborg, S.A., & Vanderlip, R.L. (1996). Sorghum grain yield reductions caused by duration and
800 timing of freezing temperatures. *Agronomy Journal, 88*, 473-477.

801   Strachan, I.B., Pattey, E., & Boisvert, J.B. (2002). Impact of nitrogen and environmental conditions on
802 corn as detected by hyperspectral reflectance. *Remote Sensing of Environment, 80*, 213-224.

803   Team, R.C. (2014). R: A language and environment for statistical computing. R Foundation for
804 Statistical Computing: Vienna, Austria.

805   Thenkabail, P.S., Smith, R.B., & Pauw, E.D. (2000). Hyperspectral vegetation indices and their
806 relationships with agricultural crop characteristics. *Remote Sensing of Environment, 71*, 158-182.

807   Thyholt, K., & Isaksson, T. (1997). Differentiation of frozen and unfrozen beef using near-infrared
808 spectroscopy. *Journal of the Science of Food and Agriculture, 73*, 525-532.

809   Tsai, F., & Philpot, W. (1998). Derivative analysis of hyperspectral data. *Remote Sensing of
810 Environment, 66*, 41-51.

811   Vapnik, V.N. (1998). Statistical learning theory. New York: Wiley-Interscience.

812   Verrelst, J., Munoz, J., Alonso, L., Delegido, J., Pablo Rivera, J., Camps-Valls, G., et al. (2012).
813 Machine learning regression algorithms for biophysical parameter retrieval: Opportunities for Sentinel-2
814 and -3. *Remote Sensing of Environment, 118*, 127-139.

815   Wang, H.f., Huo, Z.g., Zhou, G.s., Liao, Q.h., Feng, H.k., & Wu, L. (2016). Estimating leaf spad values
816 of freeze-damaged winter wheat using continuous wavelet analysis. *Plant Physiology and Biochemistry, 98*,
817 39-45.

818   Wang, H.F., Wang, J.H., Wang, Q., Miao, N.Z., Huang, W.J., Feng, H.K., et al. (2012). Hyperspectral
819 characteristics of winter wheat under freezing injury stress and LWC inversion model. First international
820 conference on agro-geoinformatics. pp. 141-146, Shanghai, China.

821   Xin, Z., & Browse, J. (2000). Cold comfort farm: The acclimation of plants to freezing temperatures.
822 *Plant Cell and Environment, 23*, 893-902.

823   Yang, X., Huang, J., Wu, Y., Wang, J., Wang, P., Wang, X., et al. (2011). Estimating biophysical
824 parameters of rice with remote sensing data using support vector machines. *Science China Life Sciences, 54*,

825   272-281.

826   Ye, X., Sakai, K., Sasao, A., & Asada, S.i. (2008). Potential of airborne hyperspectral imagery to

827   estimate fruit yield in citrus. *Chemometrics and Intelligent Laboratory Systems, 90*, 132-144.

828   Yi, Q.X., Bao, A.M., Wang, Q., & Zhao, J. (2013). Estimation of leaf water content in cotton by means

829   of hyperspectral indices. *Computers and Electronics in Agriculture, 90*, 144-151.

830   Yu, K., Lenz-Wiedemann, V., Chen, X., & Bareth, G. (2014). Estimating leaf chlorophyll of barley at

831   different growth stages using spectral indices to reduce soil background and canopy structure effects. *ISPRS*

832   *Journal of Photogrammetry and Remote Sensing, 97*, 58-77.

833   Zhai, Y.F., Cui, L.J., Zhou, X., Gao, Y., Fei, T., & Gao, W.X. (2013). Estimation of nitrogen,

834   phosphorus, and potassium contents in the leaves of different plants using laboratory-based visible and

835   near-infrared reflectance spectroscopy: Comparison of partial least square regression and support vector

836   machine regression methods. *International Journal of Remote Sensing, 34*, 2502-2518.

837   Zhang, C., Wang, T., Atkinson, P.M., Pan, X., & Li, H. (2015). A novel multi-parameter support vector

838   machine for image classification. *International Journal of Remote Sensing, 36*, 1890-1906.

839   Zhang, X., Zhang, C., Liao, X., & Wang, H. (2008). Investigation on 2008 low temperature and freeze

840   injury on winter rape along Yangtze river. *Chinese Journal of Oil Crop Sciences, 30*, 122-126.

841

842   List of Figure Captions

843   Fig. 1. Minimum and maximum daily temperatures in Hangzhou, China; (a) between

844   October 2013 and December 2013, and (b) between October 2014 and February 2015.

845   The treatment dates are indicated by gray vertical bars. Closed and open circles represent

846   maximum and minimum temperature, respectively.

847   Fig. 2. Changes of leaf temperature during freezing treatment.

848   Fig. 3. Average SPAD values of oilseed rape leaves at the normal, supercooling, 1hr of

849   freezing and at different hours of post-thawing. The bars represent ± 95% confidence

850   interval (CI) (n=26).

851   Fig. 4. Light microscopic images (a, b) and transmission electron micrographs (c, d)

852   showing transverse section of normal (a, c) and freeze-damaged (b, d) oilseed rape leaves.

853   Fig.5. Response of leaf reflectance spectra at different phases of freezing injury: (a)

854   changes in average reflectance with freezing; (b) changes in average reflectance with

855   post-thawing. N, F and PT represent normal, freezing and post-thawing in the Legend.

856   The total sample sizes are 5 and 26, respectively.

857   Fig. 6. Change in indices θ and D; (a-f) during freezing, and (g-l) post-thawing. N

858   represents normal state, F-digit denotes the duration of freezing, PT-digit means the time

859   of post-thawing. Bars represent 95% confidence interval.

860